Inorganic Chemistry
Article

*Inorg. Chem.* **2010**, *49*, 8929–8940 **8929**
DOI: 10.1021/ic101170k

# Three-Metal Coordination by Novel Bisporphyrin Architectures

**Jean-Michel Barbe,*,† Benoit Habermeyer,† Tony Khoury,†,§ Claude P. Gros,† Philippe Richard,† Ping Chen,‡ and Karl M. Kadish*,‡**

†*Université de Bourgogne, ICMUB (UMR 5260), 9, Avenue Alain Savary, BP 47870, 21078 Dijon Cedex, France, and* ‡*Department of Chemistry, University of Houston, Houston, Texas 77204-5003.* §*Present address: School of Chemistry, F11, The University of Sydney, NSW 2006, Australia*

Received June 10, 2010

The synthesis and characterization of a new type of bisporphyrin system is reported where the two macrocycles are linked in a cofacial arrangement by a substituted carbazole bridge. The three nitrogen atoms of the carbazole bridge in the compounds may complex a metal ion and thus provide a new parameter for varying the physical properties and flexibility of the dyad after formation of a three-metal system. In the present study, four bis-metalloporphyrin complexes were synthesized and examined by electrochemistry and thin-layer spectroelectrochemistry in $CH_2Cl_2$ and PhCN. Two of the examined compounds contain Cu(II) or Zn(II) porphyrins and a carbazole linker with a bound Cu(II) ion, giving a three metal system, while the other two examined compounds contained the same porphyrins but with a carbazole bridge which lacks the Cu(II) component. Since carbazoles and Cu(II) ions are both electroactive, redox properties of several unlinked carbazoles with and without bound Cu(II) ions were also examined as to their electrochemical behavior under the same solution conditions as the dyads to better understand the redox reactions which may occur at the carbazole group linking the two porphyrin macrocycles. Several mononuclear porphyrins with structures related to macrocycles in the dyads were also investigated.

## Introduction

One of the most important reactions on earth is photosynthesis. An X-ray crystal structure of the photosynthetic purple bacteria[1] led scientists to try to mimic not only the light harvesting System One (LH1) and Two (LH2) but also the photosynthetic reaction center (PRC). In the naturally occurring special pair, porphyrinic systems are involved and metalloporphyrins are therefore expected to be good candidates for artificial light harvesting systems and applications in photovoltaics, catalysis, and molecular electronics.[2]

"Pacman porphyrins" are well-known[3] and consist of two porphyrins linked in a face-to-face (cofacial) arrangement by a "rigid" bridge. Changes in the bridge structure have been used to control the distance between the two porphyrin moieties in the dyad as well as the degree of opening and closing which is directly related to changes in the extent of $\pi-\pi$ interaction between the two macrocycles and the overall properties of the compound.[4] Extensive studies have been reported in literature where cofacial metalloporphyrins have been used in the area of catalysis and energy transfer,[4,5] with the geometry of the dyad varied to optimize the desired physical requirements. Many other supramolecular assemblies involving metalloporphyrin units where metals are interacting through various types of bonding have been described and recently collected in two reviews.[6]

Herein we report the synthesis and characterization of a bisporphyrin system where the two macrocycles are linked in a cofacial arrangement by a substituted carbazole bridge as seen in Chart 1. The three nitrogen atoms of the bridge in compounds **9** and **11** may complex a metal ion and thus provide a

*To whom correspondence should be addressed. E-mail: jean-michel.barbe@u-bourgogne.fr (J.-M.B.), kkadish@uh.edu (K.M.K.).

(1) (a) McDermott, G.; Prince, S. M.; Freer, A. A.; Hawthornthwaite-Lawless, A. M.; Papiz, M. Z.; Cogdell, R. J.; Isaacs, N. W. *Nature* **1995**, *374*, 517–521. (b) Koepke, J.; Hu, X. C.; Muenke, C.; Schulten, K.; Michel, H. *Structure* **1996**, *4*, 581–597.

(2) In *The Porphyrin Handbook*; Kadish, K. M., Smith, K. M., Guilard, R., Eds.; Academic Press: Boston, 2000; Vol. *6*.

(3) (a) Chang, C. J.; Loh, Z.-H.; Deng, Y.; Nocera, D. G. *Inorg. Chem.* **2003**, *42*, 8262–8269. (b) Collman, J. P.; Hutchison, J. E.; Lopez, M. A.; Tabard, A.; Guilard, R.; Seok, W. K.; Ibers, J. A.; L'Her, M. *J. Am. Chem. Soc.* **1992**, *114*, 9869–9877. (c) Guilard, R.; Lopez, M. A.; Tabard, A.; Richard, P.; Lecomte, C.; Brandès, S.; Hutchison, J. E.; Collman, J. P. *J. Am. Chem. Soc.* **1992**, *114*, 9877–9889. (d) Rosenthal, J.; Nocera, D. G. *Prog. Inorg. Chem.* **2007**, *55*, 483–544.

(4) (a) Bolze, F.; Gros, C. P.; Drouin, M.; Espinosa, E.; Harvey, P. D.; Guilard, R. *J. Organomet. Chem.* **2002**, 89–97. (b) Gros, C. P.; Brisach, F.; Meristoudi, A.; Espinosa, E.; Guilard, R.; Harvey, P. D. *Inorg. Chem.* **2007**, *46*, 125–135. (c) Harvey, P. D.; Stern, C.; Gros, C. P.; Guilard, R. *Coord. Chem. Rev.* **2007**, *251*, 410–428. (d) Harvey, P. D.; Stern, C.; Gros, C. P.; Guilard, R. *J. Inorg. Biochem.* **2008**, *102*, 395–405. (e) Takai, A.; Gros, C. P.; Barbe, J.-M.; Guilard, R.; Fukuzumi, S. *Chem.—Eur. J.* **2009**, *15*, 3110–3122.

(5) (a) Fukuzumi, S.; Okamoto, K.; Gros, C. P.; Guilard, R. *J. Am. Chem. Soc.* **2004**, *126*, 10441–10449. (b) Fukuzumi, S.; Okamoto, K.; Tokuda, Y.; Gros, C. P.; Guilard, R. *J. Am. Chem. Soc.* **2004**, *126*, 17059–17066. (c) Gros, C. P.; Aly, S. M.; El Ojaimi, M.; Barbe, J.-M.; Brisach, F.; Abd-El-Aziz, A. S.; Harvey, P. D. *J. Porphyrins Phthalocyanines* **2007**, *11*, 244–257. (d) Tanaka, M.; Ohkubo, K.; Gros, C. P.; Guilard, R.; Fukuzumi, S. *J. Am. Chem. Soc.* **2006**, *28*, 14625–14633.

(6) (a) Beletskaya, I.; Tyurin, V. S.; Tsivadze, A. Y.; Guilard, R.; Stern, C. *Chem. Rev.* **2009**, *109*, 1659–1713. (b) Drain, C. M.; Varotto, A.; Radivojevic, I. *Chem. Rev.* **2009**, *109*, 1630–1658.


Published on Web 09/07/2010

**Chart 1.** Structures of Examined Bisporphyrins and Carbazole Linking Groups

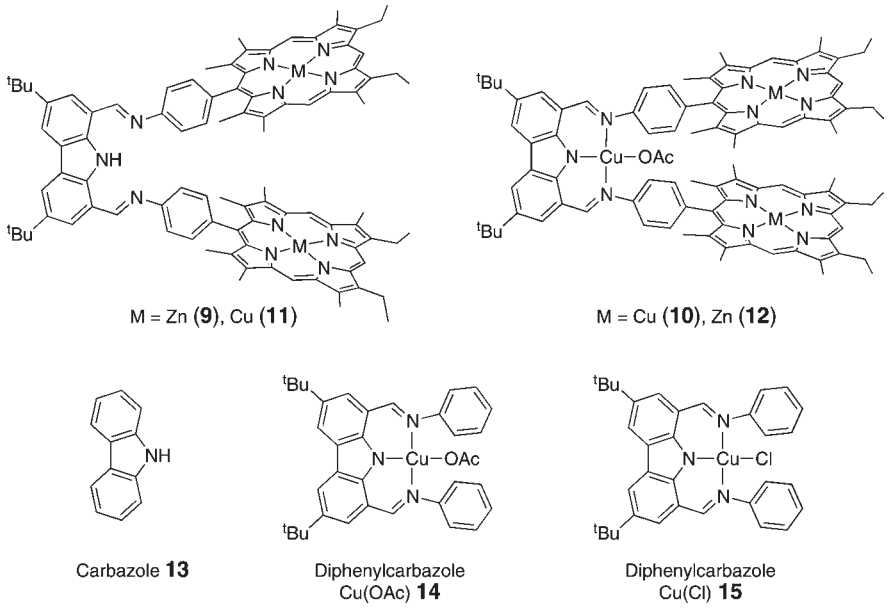


new parameter for varying the physical properties and flexibility of the dyad after formation of the three-metal systems in compounds **10** and **12**.

The four synthesized tris-metal complexes in Chart 1 were spectroscopically characterized and also examined by electrochemistry and thin-layer spectroelectrochemistry in $CH_2Cl_2$ and PhCN. Carbazoles are known to be electroactive,[7] and the three unlinked carbazoles shown in the lower part of Chart 1 were also examined as to their redox properties under the same solution conditions to better understand reactions of the dyads.

## Results and Discussion

Two different precursors are needed to obtain the desired porphyrin dimer; the first is *tert*-butyl diformylcarbazole whose synthesis was reported elsewhere;[8] the second is the amino-linker-porphyrin which is synthesized as described in Scheme 1. Direct condensation of the two separate parts leads to formation of the desired porphyrin dimer as shown in Scheme 2.

The nitro-porphyrin **3** was prepared in about 50% yield by reaction of the a,c-biladiene **1**[9] and 4-nitrobenzaldehyde **2** with a catalytic amount of *para*-toluene sulfonic acid (PTSA) in refluxing ethanol (Scheme 1). Compound **3** was reduced using tin(II) chloride dihydrate in a stirring solution of hydrogen chloride in diethyl ether (1.0 M), leading to the desired aminoporphyrin **4** in 2 h. A small quantity of chloroform was required to enhance the solubility of the porphyrin. Under these conditions, the 4-aminoporphyrin **4** was afforded in 84% yield. Metalation of **4** with zinc(II) and copper(II) was successfully achieved to give the metalated derivatives **5** and **6** in 85 and 93% yield, respectively.

The aminoporphyrin **4** (2 equiv) was reacted with diformylcarbazole **7** (1 equiv) to force condensation of the two amine functions with the two aldehyde counterparts. After refluxing a mixture of **4** and **7** in pyridine for 3 days, the bisporphyrin carbazole **8** was obtained in 85% yield (Scheme 2). The molecular weight of **8** was confirmed by the high resolution mass spectroscopy (HRMS)-electrospray ionization (ESI) spectrum, which exhibited a pseudo-molecular ion, $[M+H]^+$ at 1382.8099 Da (4 ppm deviation with respect to calculated mass).

**Scheme 1**

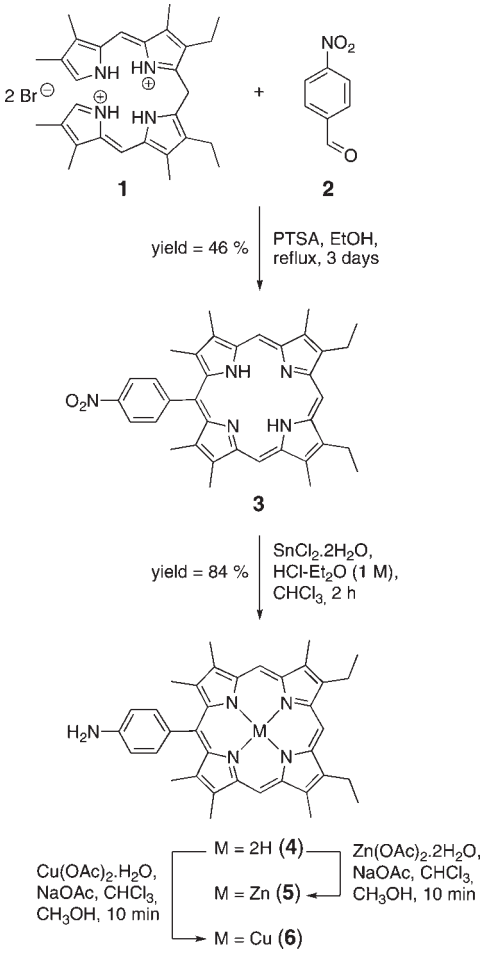


(7) (a) Ambrose, J. F.; Carpenter, L. L.; Nelson, R. F. *J. Electrochem. Soc.* **1975**, *27*, 876–894. (b) Ambrose, J. F.; Nelson, R. F. *J. Electrochem. Soc.* **1968**, *115*, 1159–1164.

(8) Gibson, V. C.; Spitzmesser, S. K.; White, A. J. P.; Williams, D. J. *Dalton Trans.* **2003**, *35*, 2718–2727.

(9) Harris, D.; Johnson, A. W.; Gaete-Holmes, R. *Biorg. Chem.* **1980**, *9*, 63–70.

**Scheme 2**

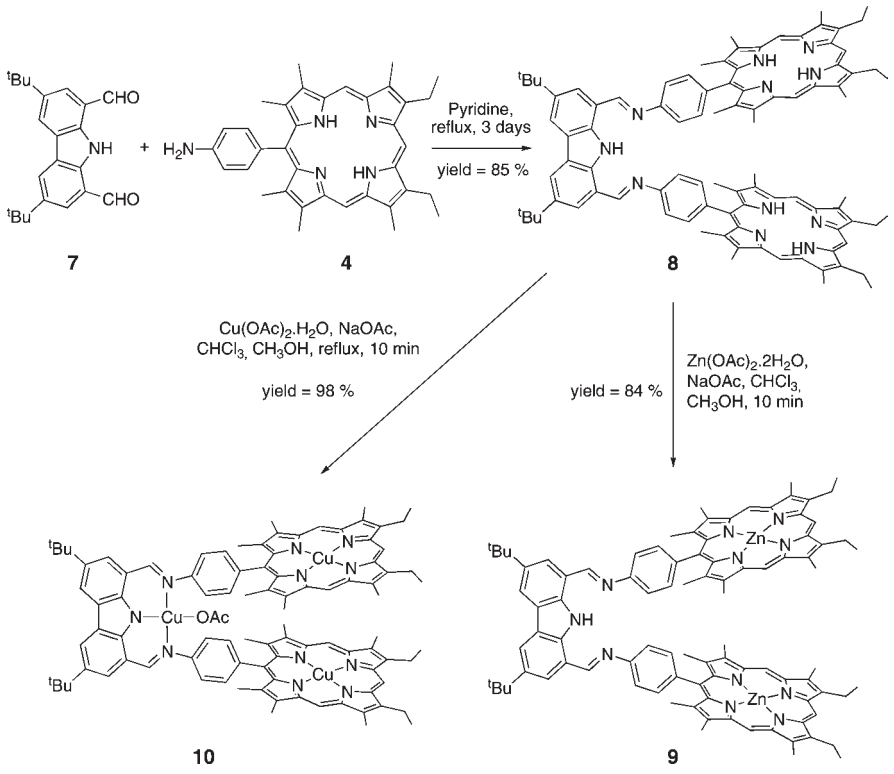


A comparison of the $^1$H NMR spectrum (in D5-py) of the free-base monoporphyrin **4** and free-base bisporphyrin carbazole **8** provides evidence that no interaction occurs between the two porphyrin macrocycles in **8** under these solution conditions. Indeed, the inner NH proton resonances appear at −2.67 ppm for **4** and −2.66 ppm for **8**. Any interaction which might have occurred would have shielded this NH proton resonance for the bisporphyrin compared to the monoporphyrin. It is noteworthy to point out that the imine bond (-C═N-) of **8** is strongly stabilized by the aromatic pathway of the molecule, and this was demonstrated by the failure of the reaction when $NaBH_4$ hydrogenation was attempted. The monoporphyrin carbazole aldehyde was concomitantly obtained in 7% yield.

Addition of Zn(II) to the two macrocycles of **8** was achieved by refluxing the bisporphyrin with zinc(II) acetate dihydrate and sodium acetate in a chloroform/methanol solution for 10 min to afford the bis-zinc(II) bisporphyrin carbazole **9** in 84% yield. In the absence of sodium acetate, the yield was decreased considerably because of acid attack of the imine bond by protons generated during the metalation process. **9** was characterized by HRMS (ESI) and $^1$H NMR (See Experimental Section).

The UV−visible absorption data for the zinc(II) aminoporphyrin **5** and the bis-zinc(II) bisporphyrin carbazole **9** are given in the Experimental Section. Nearly identical spectra are obtained for both compounds which can be explained by the minimal interaction which occurs between the two zinc(II) porphyrins in the dyad. Similarly, only minor variations in the chemical shifts are observed in the $^1$H NMR spectra of **5** or **9.** This indicates that both porphyrin macrocycles are far apart in the dyad, thus avoiding any detectable interaction.

Although zinc could not be inserted into the carbazole bridge, the metalation of **8** with copper(II) acetate in the presence of sodium acetate directly afforded the tris-copper(II) bisporphyrin carbazole **10** in 98% yield (Scheme 2). The structure of **10** was confirmed by HRMS (ESI) and matrix-assisted laser desorption/ionization-time of flight (MALDI-TOF) mass spectrometry (Supporting Information, Figure S1). The identity of the ligand bound to the Cu(II) ion in the carbazole bridge part of the molecule in **10** was not definitively proven but it is reasonably speculated to be acetate since this is the only anion employed in the reaction, and a Cu(II)OAc/Cu(I) redox process is observed as described later in the manuscript.

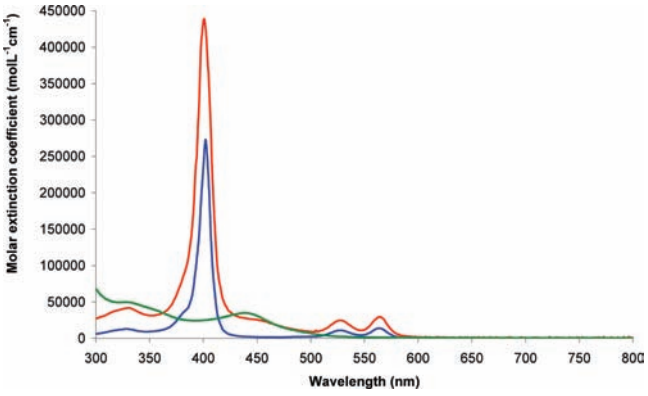


**Figure 1.** Electronic absorption spectra in $CH_2Cl_2$ of copper(II) aminoporphyrin **6** (blue), tris-copper(II) bisporphyrin carbazole **10** (red) and unlinked carbazolide copper(II) **14** (green).

The UV−visible absorption spectra of copper(II) aminoporphyrin **6** (blue), tris-copper(II) bisporphyrin carbazole **10** (red), and unlinked carbazolide copper(II) **14** (green) complexes are shown in Figure 1.

In addition to the Soret and Q bands, the spectrum of the tris-copper(II) dimer **10** possesses a broad band at about 460 nm which is not observed in the UV−vis spectrum of the monomer species **6**. This band results from an absorption of

**Scheme 3**

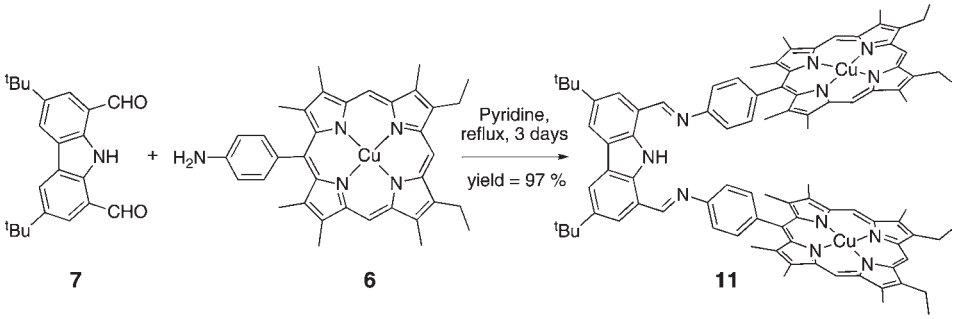


the copper carbazolide part of the molecule. Indeed, the isolated carbazole complex **14** has an absorption band at 438 nm (see Figure 1, green spectrum). Finally, UV−vis data for the neutral form seems to show that the tris-copper(II) bisporphyrin carbazole **10** behaves in solution as two separate porphyrin macrocycles without any interaction between the two $\pi$-ring systems, but this is not the case upon oxidation as described later in the manuscript. Non-interacting macrocycles in the neutral compound **10** are also observed in the solid state (See Supporting Information, Figure S2).

The direct formation of the bis-copper derivative **11** from the free-base bisporphyrin **8** using reported conditions failed since copper was also readily inserted in the carbazole bridge thus affording the tris-copper derivative **10**. Therefore, the coupling reaction of the copper amino porphyrin **6** with the carbazole aldehyde **7** was carried out in pyridine for 3 days leading to the quantitative formation of the bis-copper complex **11** (Scheme 3).

One goal of the synthesis was to prepare a dimer species incorporating two different types of metal ions and then to investigate their electrochemical, spectroscopic, and axial ligand binding properties.

Copper was chosen because of its facile coordination with the nitrogen atoms of the bridge (vide supra). The copper(II) bis-zinc(II) bisporphyrin carbazole **12** was readily obtained by refluxing a solution of the bis-zinc complex **9** with excess copper(II) acetate hydrate (Scheme 4). The formation of **12** was clearly demonstrated by MALDI-TOF and HRMS (ESI), with the appearance in the spectra of a single ionic pattern corresponding to $[M - X]^+$ (X being probably $AcO^-$) (See Experimental Section). Electron spin resonance (ESR) is a more sensitive technique than UV−visible spectroscopy to detect any interaction which might exist between the two linked copper porphyrin macrocycles of **10** and **11** in solution, and these spectra were therefore recorded at 100 K in a 1:1 $CH_2Cl_2$/toluene mixture (Figure 4). The measured $g$ tensors and coupling constants for both complexes as well as those of the monometallic copper aminoporphyrin **6** and the copper carbazole bridge analogue **14** (see Chart 1) are given in Supporting Information, Table S1.

The ESR spectrum of **11** looks like that of a classical copper(II) porphyrin with $g_{\|}$ and $g_{\perp}$ equal to 2.19 and 2.05 and $A_{\|}^{Cu}$ and $A_{\perp}^{N}$ equal to $203 \times 10^{-4}$ $cm^{-1}$ and $16.5 \times 10^{-4}$ $cm^{-1}$, respectively. The spectrum of **10**, which contains two Cu(II) porphyrin macrocycles and a Cu(II) carbazole, exhibits a less resolved signal from which only the perpendicular

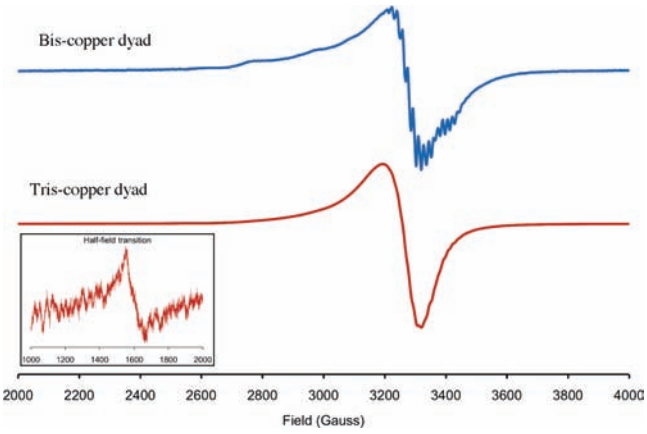


**Figure 2.** ESR spectra of bis-copper **11** (top) and tris-copper dyad **10** (bottom) at 100 K in a dichloromethane/toluene mixture 1/1. (Inset: Observed half-field transition in the tris-copper dyad **10**).

**Scheme 4**

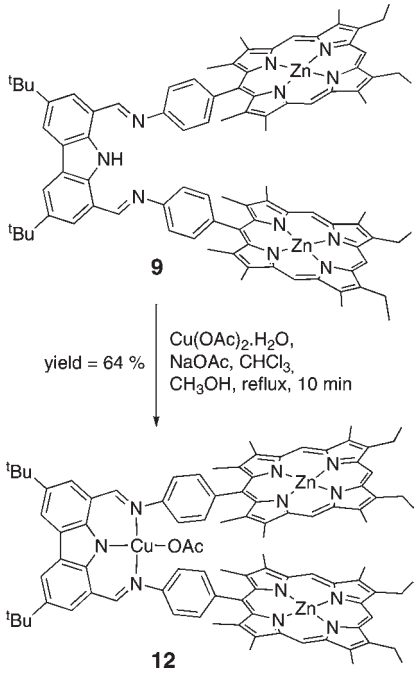


$g_{\perp}$ value of 2.06 can be undoubtedly extracted (see Figure 2 and Supporting Information, Table S1). Such a low resolution and broadened spectrum is often indicative of spin−spin interactions between two copper(II) nuclei.[10] In the present case, the contribution of the carbazolide copper part can also induce a

(10) (a) Eaton, S. S.; Eaton, G. R.; Chang, C. K. *J. Am. Chem. Soc.* **1985**, *107*, 3177–3184. (b) Suspène, C.; Brandès, S.; Guilard, R. *Chem.—Eur. J.* **2010**, DOI: 10.1002/chem.200903148; (c) Brandès, S.; David, G.; Suspène, C.; Corriu, R. L. P.; Guilard, R. *Chem.—Eur. J.* **2007**, *13*, 3480–3490.

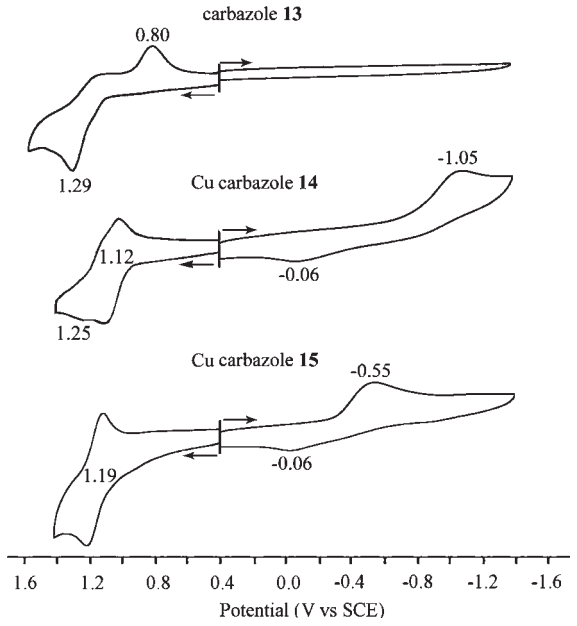


**Figure 3.** Cyclic voltammograms of the investigated carbazole derivatives **13**−**15** in $CH_2Cl_2$ containing 0.1 M TBAP.

broadening of the ESR signal. Moreover, a weak half-field signal at $g = 4.23$ is observed at low temperature (see Figure 2 inset). This signal is not detected in the spectrum of **11** or related monomer copper ($S = 1/2$) porphyrins (Supporting Information, Table S1) and can be again explained by the presence of the two interacting copper(II) nuclei of the porphyrin rings[11] in frozen solution ($S = 1$). Although intermolecular interactions cannot be absolutely ruled out as responsible for this signal, it should be noted that the approximate value of 6.8 Å calculated for the distance between the two interacting copper atoms of **10** from the intensity of the half-field ESR signal[10a,12] compares well with the separation determined from preliminary results of an X-ray structure of the chloro derivative of **10** (Supporting Information, Figures S2 and S3).

**Carbazole Electrochemistry.** Since carbazoles[7] and Cu(II) complexes[13] are known to be electroactive, redox properties of the carbazoles **13**−**15** in Chart 1 were examined as to their electrochemical behavior under the same solution conditions as the dyads **9**−**12** to better understand the redox reactions which may occur at the carbazole group linking the two porphyrin macrocycles. Several mononuclear porphyrins related to derivatives **9**−**12** were also investigated.

The electrochemical properties of the carbazoles **13**−**15** were examined in $CH_2Cl_2$ containing three types of supporting electrolytes, TBAP, TBA(OAc), and TBACl, and cyclic voltammograms in $CH_2Cl_2$, 0.1 M TBAP are illustrated in Figure 3. As seen in the figure, all three carbazoles undergo a one electron oxidation as was reported in the literature for similar compounds.[7] The unmetalated carbazole **13** is oxidized at $E_p = 1.29$ V for a scan rate of 0.1 V/s but the electro-

**Scheme 5.** Reduction Mechanisms of Cu Carbazole **14** in $CH_2Cl_2$

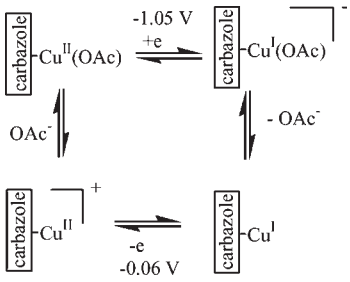


generated radical cation is unstable on the cyclic voltammetry time scale and rapidly undergoes a chemical reaction in solution as shown by the lack of a reversible process and the re-reduction peak at $E_p = 0.80$ V on the reverse potential sweep (Figure 3, top). This new reduction peak is assigned to the product of a chemical reaction following electron transfer and was not examined in further detail. However, it most likely involves a radical coupling mechanism as earlier described for related carbazoles.[7]

In contrast to the carbazole **13**, the two copper containing derivatives **14** and **15** undergo a reversible one electron oxidation at $E_{1/2} = 1.12$ (**14**) or 1.19 V (**15**) and the generated radical cations are relatively stable as seen by the cyclic voltammograms in Figure 3. Derivatives **14** and **15** also undergo an irreversible reduction at $E_p = -1.05$ V or $-0.55$ V and a re-oxidation at $E_{pa} = -0.06$ V in both cases. The reductions are both assigned to the Cu(II)/Cu(I) process of bound CuX where $X = OAc^-$ (**14**) or $Cl^-$ (**15**) and the re-oxidation, which is not observed in the cyclic voltammogram of unmetalated **13**, is assigned to the Cu(I)/Cu(II) reaction of the product where the electrogenerated Cu(II) on the return sweep is assigned to a species which is either uncomplexed or coordinated by a $ClO_4^-$ ion from the TBAP supporting electrolyte on the electrochemical time scale.

This reduction of Cu(II) remains irreversible for both **14** and **15** when the temperature of the $CH_2Cl_2$ solution was lowered to $-70$ °C, indicating an extremely rapid chemical reaction following electron transfer, and this electrochemical EC mechanism is proposed to involve the rapid loss of $OAc^-$ or $Cl^-$ after generation of Cu(I). The fact that the reverse Cu(I)/Cu(II) anodic process occurs at $E_p = -0.06$ V for both compounds indicates that neither $Cl^-$ nor $OAc^-$ is involved in the re-oxidation step. However, the lack of a reduction coupled to process at $-0.06$ V also suggests an electrochemical EC (electron transfer with following chemical reaction) mechanism on the re-oxidation and the rapid binding of $Cl^-$ or $OAc^-$ after generation of Cu(II) to give the original $Cu^{II}X$ species at the electrode surface.

It should also be pointed out that the much more negative Cu(II)/Cu(I) reduction potential of the acetate bound species (**14**), as compared to the chloride bound derivative (**15**) is consistent with a much stronger Cu(II) binding constant for $OAc^-$ in **14** than for $Cl^-$ in **15**; in fact the 500 mV difference in peak potentials between the two processes ($-1.05$ vs $-0.55$ V) is consistent with a difference in formation constants of approximately 10 orders of magnitude (assuming a $-59$ mV shift in $E_p$ for each 10-fold increase in log $K$).

In summary, the irreversible reduction at $-1.05$ (**14**) or $-0.55$ V (**15**), coupled with the irreversible re-oxidation at $-0.06$ V is consistent with two separate electrochemical EC mechanisms as shown in Scheme 5 for the case of **14** and

(11) (a) Blondin, G.; Frapart, Y.-M. *L'Actualité Chimique* **1996**, *7*, 112–124. (b) Drago, R. S. *Physical Methods in Chemistry*; 1st ed.; W.B. Saunders Company: Philadelphia, 1977.

(12) Eaton, S. S.; More, K. M.; Sawant, B. M.; Eaton, G. R. *J. Am. Chem. Soc.* **1983**, *105*, 6560–6567.

(13) (a) Hartman, J. A. R.; Kammier, A. L.; Spracklin, R. J.; Pearson, W. H.; Combariza, M. Y.; Vachet, R. W. *Inorg. Chim. Acta* **2004**, *357*, 1141–1151. (b) Rybak-Akimova, E. V.; Nazarenko, A. Y.; Chen, L.; Krieger, P. W.; Herrera, A. M.; Tarasov, V. V.; Robinson, P. D. *Inorg. Chim. Acta* **2001**, *324*, 1–15.

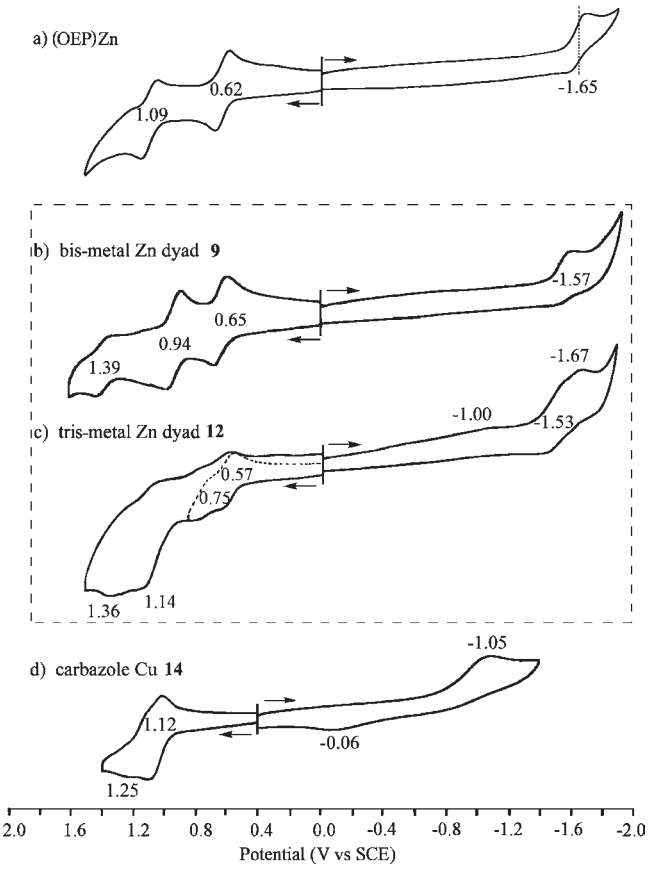


**Figure 4.** Cyclic voltammograms of (a) (OEP)Zn, (b) bis-metal Zn dyad **9**, (c) tris-metal Zn dyad **12**, and (d) diphenylcarbazole Cu(OAc) **14** in $CH_2Cl_2$ containing 0.1 M TBAP.

described above for both **14** and **15**. As will be demonstrated later in the manuscript, the same Cu(II)/Cu(I) reactions occur upon reduction of **10** and **12**, all of which contain Cu(II) bound to $OAc^-$ in the carbazole bridge.

**Electrochemistry of Tris-Metal and Bis-Metal Dyads.** The electron transfer reactions of the investigated dyads can occur at the conjugated $\pi$-ring system of the two porphyrin macrocycles and at the electroactive carbazole bridge. The exact site of electron transfer will depend upon the presence or absence of Cu(II) in the carbazole bridge and can be assigned, with some degree of certainty by comparing oxidation and reduction potentials for the individual redox active parts of the molecule when measured outside of the dyad. An example of this is given in Figure 4, which compares cyclic voltammograms of the dyads **9** and **12** in $CH_2Cl_2$ with that of (OEP)Zn which is used as a monomeric porphyrin in place of $(Et_2Me_6PhP)Zn$ and the unlinked Cu carbazole **14** under the same solution conditions. The measured $E_{1/2}$ values for the first oxidation and first reduction of OEP and the $Et_4Me_4PhP$, $Et_2Me_6PhP$, or $Et_6Me_2PhP$ derivatives with a given central metal ion (Zn,[4e] Co,[14] or Cu[15]) are almost identical within experimental error in $CH_2Cl_2$. This suggests a negligible substituent effect of the single phenyl group at one *meso*-position of the three $(Et_xMe_yPhP)M$ derivatives where $x + y = 8$ and allows for the use of (OEP)M as a comparison compound in place of $(Et_xMe_yPhP)M$ when the desired monomeric porphyrin is not available for study.

The two ring-centered oxidations of (OEP)Zn ($E_{1/2}$ = 0.62 and 1.09 V) are separated by 370 mV in potential and this compares to a 290 mV separation in $E_{1/2}$ between the two ring-centered oxidations of the bis-metal dyad **9** ($E_{1/2}$ = 0.65 and 0.94 V). As seen from Figure 4, the first oxidation of **9** is harder than the first oxidation of (OEP)Zn by 30 mV while the first reduction of **9** is easier by 80 mV than the first reduction of (OEP)Zn. The exact potentials for each redox processes of these compounds are given in the Table 1.

The gap between the highest occupied molecular orbital (HOMO) and the lowest unoccupied molecular orbital (LUMO) of (OEP)Zn is 2.27 V which compares to 2.22 V in the case of **9**. There is also a reversible third oxidation of **9** at $E_{1/2}$ = 1.39 V whose peak current is approximately half that of the first two oxidations. This suggests half as many electrons are abstracted at $E_{1/2}$ = 1.39 V as compared to the reactions at 0.65 or 0.94 V which involve the two linked macrocycles each undergoing a one electron transfer. The relative peak currents are also consistent with a one-electron abstraction from the carbazole part of dyad which also occurs in the case of the unlinked carbazoles **13**−**15** (Figure 3).

It is important to point out that no "splitting" of half wave potentials is observed for the two oxidation peaks of **9** as would be expected for electrode reactions involving two equivalent and interacting redox centers.[16] The electrochemical data thus clearly indicates that two *non-interacting* redox centers are involved in the electron transfer processes at 0.65 or 0.94 V. Under these conditions, each oxidation of **9** must involve an overlapping of two one-electron abstractions at the same potential, one at each Zn porphyrin unit to give first a dyad with two linked porphyrin $\pi$ cation radicals and then, after the second oxidation, another dyad with two linked porphyrin dications. The last electron transfer of **9** at $E_{1/2}$ = 1.39 V involves a one electron abstraction and must occur at the carbazole bridge as described earlier in the manuscript for unlinked carbazoles with similar structures to those in the dyads.

Quite different electrochemical behavior is seen for the tris-metal Zn dyad **12** which contains Cu(II) in the carbazole bridge. Unlike the case of **9** which shows no interaction between redox centers under the electrochemical solution conditions, the first oxidation of **12** is split into two processes of approximately equal height at $E_{1/2}$ = 0.57 and 0.75 V, consistent with an interaction between the two redox active sites of the porphyrin in the tris-metal dyad. Thus, the presence of a Cu(II) ion in the carbazole bridge must contribute to an enhanced $\pi-\pi$ interaction between the two porphyrin macrocycles, as is also suggested by the low temperature ESR data described earlier in the manuscript for the same tris-Cu dyad.

Additional oxidations beyond the initial split peaks of **12** are ill-defined and located at $E_p$ = 1.14 and 1.36 V as

(14) (a) Kadish, K. M.; Frémond, L.; Shen, J.; Chen, P.; Ohkubo, K.; Fukuzumi, S.; El Ojaimi, M.; Gros, C. P.; Barbe, J. M.; Guilard, R. *Inorg. Chem.* **2009**, *48*, 2571–2582. (b) Zhu, W. H.; Zhao, X. F.; Ou, Z. P.; Zhou, F.; Wang, X. H.; Kadish, K. M. *J. Porphyrins Phthalocyanines* **2009**, *13*, 1233–1242.

(15) Guilard, R.; Gros, C. P.; Barbe, J.-M.; Espinosa, E.; Jérôme, F.; Tabard, A.; Latour, J.-M.; Shao, J.; Ou, Z.; Kadish, K. M. *Inorg. Chem.* **2004**, *43*, 7441–7455.

(16) (a) Guilard, R.; Barbe, J.-M.; Stern, C.; Kadish, K. M. In *The Porphyrin Handbook*; Kadish, K. M., Smith, K. M., Guilard, R., Eds.; Academic Press: San Diego, 2003; Vol. *18*, pp 303−349; (b) Le Mest, Y.; L' Her, M.; Saillard, J.-Y. *Inorg. Chim. Acta* **1996**, *248*, 181–191. (c) Le Mest, Y.; L'Her, M.; Courtot-Coupez, J.; Collman, J. P.; Evitt, E. R.; Bencosme, C. S. *J. Electroanal. Chem.* **1985**, *184*, 331–346. (d) Le Mest, Y.; L'Her, M.; Hendricks, N. H.; Kim, K.; Collman, J. P. *Inorg. Chem.* **1992**, *31*, 835–847.

**Table 1.** Half-Wave and Peak Potentials (V versus SCE) for Reduction of Zn Dyads and Related Carbazoles in $CH_2Cl_2$ Containing 0.1 M TBAX Where X = $ClO_4^-$, $Cl^-$, or $OAc^-$

| | | bridge | | porphyrin | | |
|---|---|---|---|---|---|---|
| anion of supporting electrolyte | compound | Cu (II)/Cu(I) | | 1st | 2nd | $\Delta^b$ (V) |
| $ClO_4^-$ | bis-metal Zn **9** | none | | −1.57 | | |
| | tris-metal Cu−Zn **12** | −1.00[a] | | −1.53 | −1.67[a] | 0.14 |
| | carbazole Cu **14** ($OAc^-$) | −1.05[a] | | | | |
| | carbazole Cu **15** ($Cl^-$) | −0.55[a] | | | | |
| $Cl^-$ | bis-metal Zn **9** | none | | −1.55[a] | −1.70[a] | 0.15 |
| | tris-metal Cu−Zn **12** | −0.60[a] | | −1.41 | −1.60[a] | 0.19 |
| | carbazole Cu **14** ($OAc^-$) | −0.68[a] | −0.90[a] | | | |
| $OAc^-$ | bis-metal Zn **9** | none | | −1.68[a] | −1.75[a] | 0.07 |
| | tris-metal Cu−Zn **12** | −0.90[a] | | −1.45 | −1.72[a] | 0.27 |
| | carbazole Cu **15** ($Cl^-$) | −0.93[a] | | | | |

[a] Peak potential at a scan rate of 0.1 V/s. [b] $\Delta$ = potential difference between two reductions.

seen in Figure 4. These processes involve overlapping macrocycle and bridge-centered oxidations.

Two other features should be pointed out as significant in the cyclic voltammogram of **12**. The first is the presence of a broad reduction peak at $E_p \approx -1.00$ V and the second a "new" peak at $E_p = -1.67$ V, neither of which is observed in cyclic voltammograms of (OEP)Zn or the bis-metal Zn dyad **9**. Both of these "new" redox processes in **12** are associated with the Cu(II)/Cu(I) reaction of the bridge, the first directly and the second indirectly as described below.

The most obvious evidence for assigning the broad redox process at $E_p \approx -1.00$ V to a Cu(II) reduction in the tris-metal Zn dyad **12** comes from comparison with the unlinked copper carbazole **14** which is irreversibly reduced at $E_p = -1.05$ V under the same experimental conditions in $CH_2Cl_2$ (see Figure 3). Additional evidence for the Cu(II)/Cu(I) reduction of **12** comes from spectroelectrochemical data of the type shown in Figure 5 which presents UV−vis spectra of the Cu carbazole **14** and the tris-metal Zn dyad **12** as the reductions are carried out under a controlled applied potential in PhCN.

As the first reduction of the carbazole **14** proceeds at an applied potential of −1.20 V in PhCN, the band at 444 nm decreases in intensity and shifts to 450 nm as two absorptions grow up at 329 and 487 nm (Figure 5a). These changes are associated with the conversion of Cu(II) to Cu(I), the only reduction which occurs in compound **14** up to the negative potential limit of the solvent. Similar spectral changes are observed for reduction of the tris-metal Zn **12** (Figure 5b), and this suggests the same copper-centered electrode reaction in both compounds. Finally, when the controlled potential for reduction of **12** is switched from −1.20 to −1.70 V (Figure 5c), the Soret band at 409 nm decreases substantially in intensity while a broad and weak visible band appears at 754 nm, indicating formation of a porphyrin $\pi$-anion radical.[17]

Of some significance when comparing the cyclic voltammograms of **9** and **14** in Figure 4 is the fact that the porphyrin ring-centered reduction, which appears as a single process at $E_{1/2} = -1.57$ V in **9**, is split into two processes in **12**, one of which is located at $E_{1/2} = -1.53$ V and the other at $E_p = -1.67$ V in $CH_2Cl_2$ containing 0.1 M TBAP. Because only one porphyrin-centered reduction is observed for **9** under the same solution conditions, the "extra" process of **12** could be

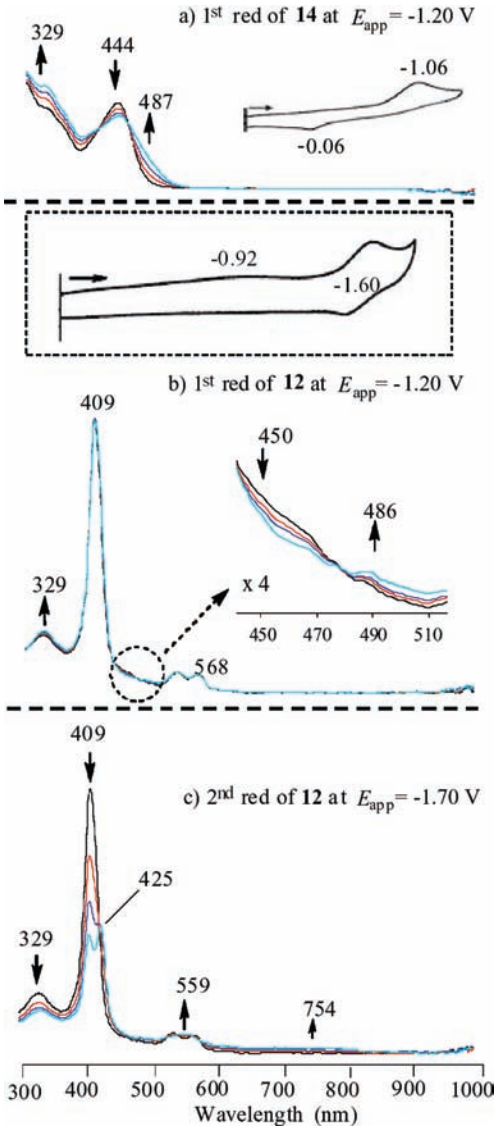


**Figure 5.** UV−vis spectral changes for (a) diphenylcarbazole Cu **14** during controlled potential reduction at −1.20 V (see CV in inset), (b) tris-metal Zn dyad **12** during reduction at the same potential (see CV on the top of spectral changes) and (c) **12** during further reduction at −1.70 V in PhCN containing 0.2 M TBAP.

rationalized as resulting from two possibilities. The first one is the interaction between two macrocycles and the second is two different forms of the Zn(II) porphyrin in the tris-metal dyad. The latter is proposed where one of two porphyrins in

(17) (a) Fuhrhop, J. H. *Struct. Bonding* (*Berlin*) **1974**, *18*, 1–67. (b) Gouterman, M. *J. Mol. Spectrosc.* **1961**, *6*, 138–163. (c) Perrin, M. H.; Gouterman, M.; Perrin, C. L. *J. Chem. Phys.* **1969**, *50*, 4137–4151.

**Scheme 6.** Reductions of Tris-Metal Zn Dyad **12** in $CH_2Cl_2$ Containing 0.1M TBAP

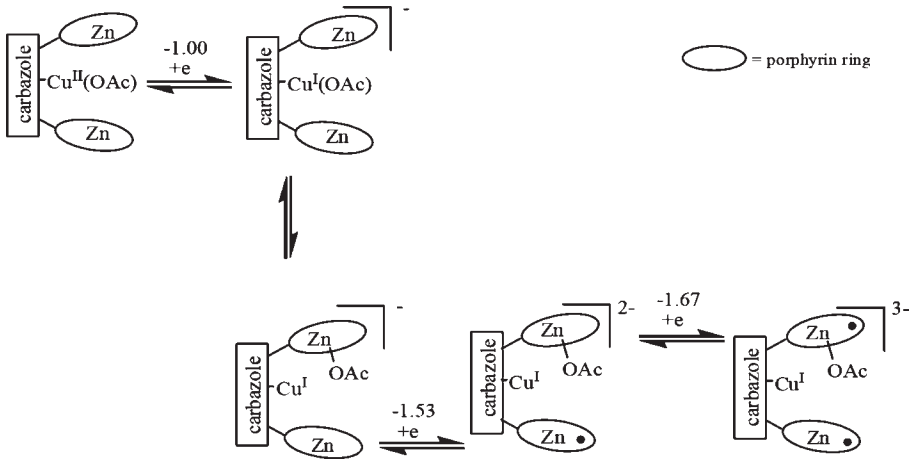


the dyad contains an uncoordinated Zn(II) center while the second one contains Zn(II) with the axially coordinated $OAc^-$ anion that is liberated from Cu(II) after electroreduction at the bridge part of the molecule. To clarify this point, compounds **9** and **12** as well as (OEP)Zn were selected for examining their anion binding properties with both $OAc^-$ and $Cl^-$ added in the form of TBAX where X is the anion.

A summary of reduction potentials for the linked porphyrins **9**, **12** with the unlinked bridges **14** and **15** in $CH_2Cl_2$ containing 0.1 M of different supporting electrolytes is given in Table 1, and examples of the cyclic voltammograms under these conditions are shown in Supporting Information, Figures S4 and S5 for **9** and **12**. As seen in Table 1, the potential difference between the two split reduction processes of **12** to give the porphyrin $\pi$ anion radical range from 0.14 V in $CH_2Cl_2$ containing 0.1 M TBA($ClO_4$) to 0.27 V in the same solvent containing 0.1 M TBA(OAc) as supporting electrolyte. Split reduction processes are also observed for **9** in $CH_2Cl_2$ containing 0.1 M TBACl and TBA(OAc), and this suggests two different axially coordinated forms of the linked Zn porphyrin macrocycles, each of which has a different reduction potential.

The proposed mechanism for reduction of the tris-metal Zn dyad **12** in $CH_2Cl_2$ containing 0.1 M TBAP is shown in Scheme 6, where the first reduction at −1.00 V (Figure 4c) involves the Cu(II)/Cu(I) reaction of the carbazole bridge. This scheme is similar to the one shown in Scheme 5 for the unlinked carbazole but in the case of the porphyrin, the $OAc^-$ ion which dissociates from $Cu^{II}(OAc)^-$ can then axially bind to one of the two Zn porphyrin centers, thus leading to a negative shift in the measured $E_{1/2}$ value for formation of the porphyrin $\pi$ anion radical.

A splitting of the redox process for the $\pi$-anion radical formation of compound **12** is due to the binding of $OAc^-$ by only one of the two metalloporphyrin centers and is specific to the $Zn^{II}$ complexes since acetate does not strongly bind to the $Cu^{II}$.

It is interesting to point out that while no interaction is observed for the neutral singly oxidized or doubly oxidized bis-Zn porphyrin dyad **9** (Figure 5b), this is not the case for the bis-Cu porphyrin dyad **11** with the same macrocycle where both oxidations are split into two well-defined processes, the first at $E_{1/2} = 0.72$ and 0.89 V and the second at 1.15 and 1.26 V as seen in Figure 6b. This behavior is quite different than that of ($Me_2Et_6PhP$)Cu which shows

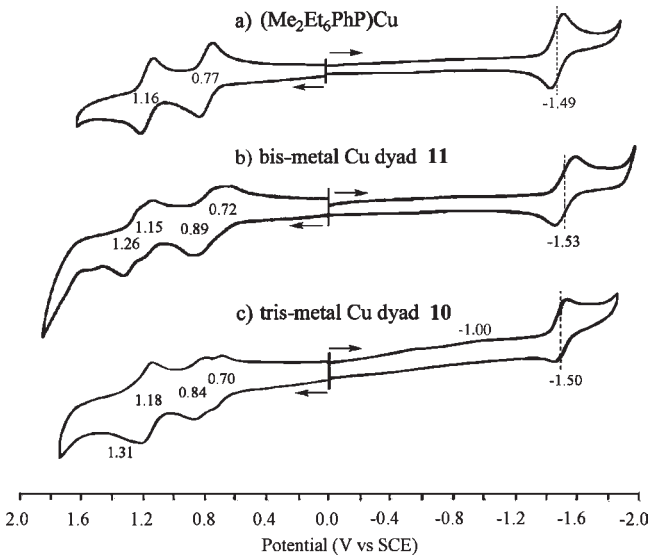


**Figure 6.** Cyclic voltammograms of (a) ($Me_2Et_6PhP$)Cu, (b) bis-metal Cu dyad **11**, and (c) tris-metal Cu dyad **10** in $CH_2Cl_2$ containing 0.1 M TBAP. Data on the ($Me_2Et_6PhP$)Cu are taken form ref 15.

well-defined one electron oxidation at 0.77 and 1.16 V (Figure 6a).

The reason for the difference in electrochemical behavior between the structurally related Zn dyad **9** and Cu dyad **11** is unknown, but it should also be pointed out that the tris-metal Cu dyad **10** also shows an interaction upon oxidation, and this can only occur if a large structure rearrangement occurs after the abstraction of one electron (see X-ray view of neutral molecule of **10** in Supporting Information, Figure S2). Little to no separation is seen for the second oxidation, which occurs at $E_{1/2} = 1.18$ V (Figure 6c) and maybe overlapped with an oxidation of the carbazole bridge.

**Effect of the Third Coordinated Metal on Ligand Binding Properties of Zn Dyads.** The axial ligand binding properties of monomeric Zn porphyrins have been well studied in non-aqueous media.[18] Only a five-coordinate

(18) (a) Kadish, K. M.; Van Caemelbecke, E.; Royal, G. In *The Porphyrin Handbook*; Kadish, K. M., Smith, K. M., Guilard, R., Eds.; Academic Press: San Diego, 2000; Vol. *8*, pp 1−260; (b) Kadish, K. M.; Rhodes, R. K. *Inorg. Chem.* **1981**, *20*, 2961–2966. (c) Tabata, M.; Nishimoto, J. In *The Porphyrin Handbook*; Kadish, K. M., Smith, K. M., Guilard, R., Eds.; Academic Press: San Diego, 2000; Vol. *9*, pp 222−413.

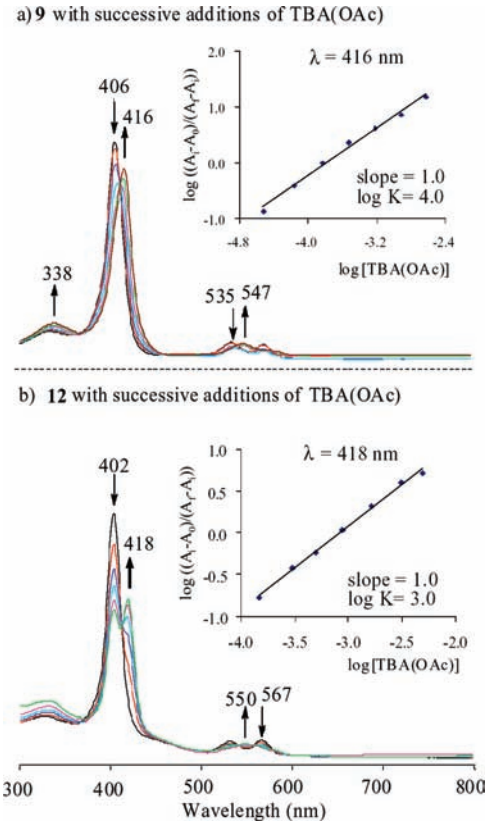


**Figure 7.** UV−vis spectral change of (a) $8.40 \times 10^{-6}$ M bis-metal Zn dyad **9** with 0−300 equiv of TBA(OAc) in $CH_2Cl_2$. (inset shows the Hill plot) and (b) $7.60 \times 10^{-6}$ M tris-metal Zn dyad **12** with 0−9000 equiv of TBA(OAc) in $CH_2Cl_2$ (inset shows the Hill plot).

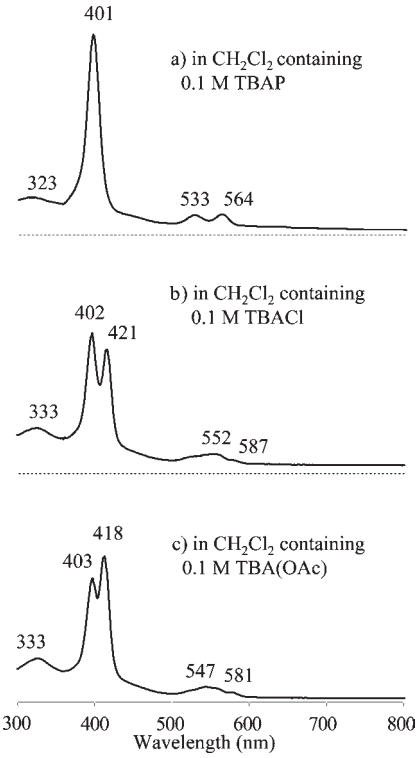


**Figure 8.** UV−vis spectra of tris-metal Zn dyad **12** ($\sim 10^{-6}$ M) in $CH_2Cl_2$ solutions containing 0.1 M TBAX where X = $ClO_4^-$, $Cl^-$, or $OAc^-$.

complex is formed, and the same is expected for the dyads where each $Zn^{II}$ center can bind at most one axial ligand.

In the present study, binding constants of $Cl^-$ and $OAc^-$ with the Zn dyads **9** and **12** were measured in $CH_2Cl_2$, and the progress of the reaction was followed by UV−visible spectroscopy. An example of the spectral changes for **9** and **12** with successive additions of TBA(OAc) to the $CH_2Cl_2$ solution is shown in Figure 7. As seen in this figure, successive additions of $OAc^-$ to a $CH_2Cl_2$ solution of **9** leads to red shift of the Soret band from 406 to 416 nm. There are also multiple well-defined isosbestic points in the spectra. The Soret bands at 406 and 416 nm correspond to the unligated and ligated species, respectively. The changes in absorbance at 416 nm were analyzed as a function of added $OAc^-$ concentration, and a diagnostic plot of $\log((A_i - A_0)/(A_f - A_i))$ versus $\log[OAc^-]$ gave a slope of 1.0 with a zero intercept of 4.0, indicating that one $OAc^-$ molecule is bound to each zinc center of the dyad with a formation constant of $10^4$.

As mentioned earlier in the manuscript, an interaction between two redox centers of the macrocycle **9** is negligible upon reduction and the two porphyrin units are reduced independent of each other, like a monomer with double the concentration. This being the use, one would expect each zinc center to bind one $OAc^-$ with $\log K = 4.0$.

In contrast to above, the binding of $OAc^-$ to **12**, however, is quite different than in the case of **9** or (OEP)Zn (see Supporting Information, Figure S6). For this dyad, the UV−visible spectrum in $CH_2Cl_2$ solution with excess acetate exhibits bands at both 402 and 418 nm, suggesting that $OAc^-$ is bound to only one of the two Zn centers of the dyad. The spectral changes upon addition of $OAc^-$ to a $CH_2Cl_2$ solution of **12** (see Figure 7b) shows that the Soret band at 402 nm loses intensity but does not disappear as a second Soret band at 418 nm at the end of the reaction. Both the 402 and 418 nm bands have approximately half the intensity of the initial Soret band at 402 nm which might suggest that one Zn porphyrin is not axially ligated. Similar spectral changes were obtained in the reactions of **12** with $Cl^-$, and the spectra obtained as a function of increasing ligand concentration are given in Supporting Information, Figure S7.

The unligated species also seems to be present in $CH_2Cl_2$ solution containing high concentrations of the ligand, thus suggesting that one of the Zn centers remains four-coordinate. As shown in Figure 8, a certain amount of the unbound **12** (402−403 nm) and bound (417−421 nm) are simultaneously present in $CH_2Cl_2$ with 0.1 M added $Cl^-$ or $OAc^-$, but no such spectral behavior is seen for **9** or (OEP)Zn under the same solution conditions (see Supporting Information, Figures S8 and S9). Moreover, the porphyrin-centered reduction of **12** occurs *via* two separate processes in $CH_2Cl_2$ containing $Cl^-$ or $OAc^-$ (see Supporting Information, Figures S4 and S5) also suggesting a different degree of axial ligand binding to each macrocycle under the electrochemical conditions.

The Hill plot in Figure 7b gives a slope of 1.0 with an intercept of 3.0, implying the binding of an $OAc^-$ axial ligand to one of two zinc centers of **12** with $\log K = 3.0$. The proposed mechanism for binding of $Cl^-$ or $OAc^-$ to the Zn dyads **9** and **12** is presented in Scheme 7.

Table 2 summarizes binding constants of the bis-metal and tris-metal Zn dyads with axial ligands. As compared to the bis-metal dyad, the binding constants are obviously smaller in the case of the tris-metal dyad. As mentioned earlier, the presence of a third metal ion in the carbazole

**Scheme 7.** Binding Reaction of Zn Dyads with Ligands

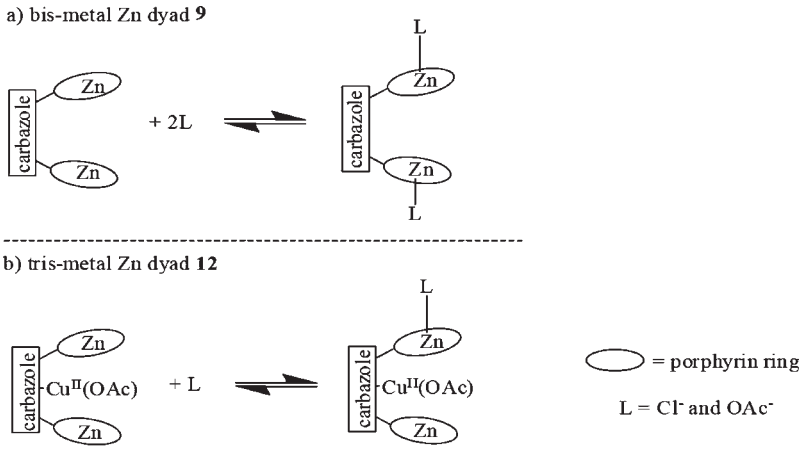


**Table 2.** Binding Constants (log $K$) of Zn Dyads in $CH_2Cl_2$

| ligand | bis-metal dyad **9** | tris-metal dyad **12** |
|---|---|---|
| $Cl^-$ | 2.2 | 1.6 |
| $OAc^-$ | 4.0 | 3.0 |

bridge decreases the distance between the two macrocycles and enhances their interaction. As a result, the binding ability of the Zn porphyrin with axial ligands is weakened while the number of axial ligands is reduced.

## Experimental Section

**Materials.** 1,19-Dideoxy-8,12-diethyl-2,3,7,13,17,18-hexamethylbiladien-a,c dibromide **1**, 1,8-diformyl-3,6-di-*tert*-butyl-carbazole and 1,8-diphenylimino-3,6-di-*tert*-butylcarbazole were synthesized according to previously reported procedures.[8,9] Absolute dichloromethane ($CH_2Cl_2$, Fluka Chemical Co.), pyridine (py, 99.8%, Aldrich Co), and 4,4′-dipyridyl (dipy, 98%, Aldrich Co) were used as received. Benzonitrile (PhCN) was purchased from Aldrich Chemical Co. and distilled over $P_2O_5$ under vacuum prior to use. Tetra-*n*-butylammonium perchlorate (TBAP), tetra-*n*-butylammonium chloride (TBACl, 97%), and tetra-*n*-butylammonium acetate ((TBA)OAc, 99%) were obtained from Fluka Chemical Co. and dried under vacuum at 30 °C for at least 1 week prior to use.

**Instrumentation.** $^1$H NMR spectra for synthesized compounds were recorded on a Bruker DRX-300 AVANCE spectrometer at the "Plateforme d'Analyse Chimique et de Synthèse Moléculaire de l'Université de Bourgogne (PACSMUB)". Chemical shifts are expressed in parts per million (ppm) relative to chloroform (7.26 ppm) or D5-pyridine (7.22, 7.58, and 8.74 ppm). The mass spectra were obtained on a Bruker Daltonics Ultraflex II spectrometer at the PACSMUB in the MALDI/TOF reflectron mode using dithranol as a matrix. High resolution mass measurements (HR-MS) were carried out in the same conditions as previously (Bruker Daltonics Ultraflex II) using PEG ion series as internal calibrant or on a Bruker Micro-ToF Q instrument in ESI mode. The UV−visible spectra were recorded on a Varian Cary 1 spectrophotometer. Cyclic voltammetry was carried out with an EG&G Princeton Applied Research (PAR) 173 potentiostat/galvanostat. A homemade three-electrode cell was used for cyclic voltammetric measurements and consisted of a glassy carbon working electrode, a platinum counter electrode, and a homemade saturated calomel reference electrode (SCE). UV−visible spectroelectrochemical experiments were performed with a home-built thin-layer cell that had a light transparent platinum net working electrode.[19] Potentials were applied and monitored with an EG&G PAR Model 173 potentiostat. Time-resolved UV−visible spectra were recorded with a Hewlett-Packard Model 8453 diode array spectrophotometer.

**Synthesis of 13,17-Diethyl-2,3,7,8,12,18-hexamethyl-5-*p*-nitrophenylporphyrin 3.** A solution of 1,19-dideoxy-8,12-diethyl-2,3,7,13,17,18-hexamethylbiladien-a,c dibromide **1** (398 mg, 0.66 mmol) and 4-nitrobenzaldehyde **2** (996 mg, 6.59 mmol) in 5 mL of absolute ethanol was refluxed under nitrogen in a two-neck round-bottom flask equipped with a condenser, a magnetic stirrer, and shielded from light. To this mixture was added dropwise (1 h) a solution of recrystallized *p*-toluenesulfonic acid (PTSA) (802 mg, 4.66 mmol) in 2 mL of absolute ethanol. After 3 days of reflux, the reaction mixture was cooled to room temperature and extracted with 100 mL of chloroform. The organic layer was then washed three times with water, dried over magnesium sulfate and evaporated. The solid residue was then chromatographed over silica gel and eluted with chloroform. The first brown band was collected affording the pure porphyrin **3** (173 mg, 46%). An analytically pure sample was obtained by recrystallization from a chloroform/methanol solution. UV−vis ($CH_2Cl_2$) 398 (log $\varepsilon$, 4.95), 501 (3.89), 533 (3.68), 569 (3.54), 622 (3.32) nm.$^1$H NMR (300 MHz, $CDCl_3$) $\delta$ (ppm): −3.31 (s, 1 H, inner NH); −3.22 (s, 1 H, inner NH); 1.88 (t, $J$ = 7.3 Hz, 6 H, $CH_2\underline{CH_3}$); 2.38 (s, 6 H, $CH_3$); 3.52 (s, 6 H, $CH_3$); 3.64 (s, 6 H, $CH_3$); 4.03−4.11 (q, $J$ = 7.3 Hz, 4 H, $\underline{CH_2}CH_3$); 8.20 (d, $J$ = 8.6 Hz, 2 H, aryl-H); 8.57 (d, $J$ = 8.6 Hz, 2 H, aryl-H); 9.98 (s, 1 H, *meso*-15 H); 10.17 (s, 2 H, *meso*-10, *meso*-20 H). MS (MALDI-TOF): $m/z$ = 572.07 $[M+H]^+$; 572.30 calcd for $C_{36}H_{38}N_5O_2$. HRMS (ESI) $m/z$ = 572.3069 $[M+H]^+$; 572.3020 calcd for $C_{36}H_{38}N_5O_2$; $m/z$ = 1143.6011 $[2M+H]^+$. 1143.5967 calcd for $C_{72}H_{75}N_{10}O_4$.

**Synthesis of 13,17-Diethyl-2,3,7,8,12,18-hexamethyl-5-*p*-aminophenylporphyrin 4.** Nitrophenylporphyrin **3** (0.52 g, 0.90 mmol) was dissolved in chloroform (15 mL), and a hydrochloric acid/ether mixture (1 M, 35 mL) of tin(II) chloride dihydrate (3.22 g, 14.27 mmol) was added. The solution was stirred in the dark for 4 h. The reaction mixture was poured onto ice (50 g) and when the ice melted, chloroform (40 mL) was added. The organic layer was washed with water (300 mL), sodium carbonate solution (10%, 200 mL), water (200 mL), and dried over magnesium sulfate. The solvent was then removed, and the crude product was purified by column chromatography over silica (dichloromethane/methanol; 100:5). The first red band was collected leading to aminophenylporphyrin **4** (0.41 g, 84%) as a red microcrystalline solid. UV−vis ($CH_2Cl_2$) 371sh (log $\varepsilon$, 4.89), 404 (5.35), 503 (4.26), 535 (3.80), 571 (3.80), 624 (3.32) nm. $^1$H NMR (300 MHz, $CDCl_3$) $\delta$ (ppm): −3.26 (s, 2 H, inner NH); 1.88 (t, $J$ = 7.5 Hz, 6 H, $CH_2\underline{CH_3}$); 2.58 (s, 6 H, $CH_3$); 3.53 (s, 6 H, $CH_3$); 3.64 (s, 6 H, $CH_3$); 4.03−4.11 (q, $J$ = 7.5 Hz, 4 H, $\underline{CH_2}CH_3$ overlapped with br s, 2 H, $NH_2$); 7.05 (d, $J$ = 8.3 Hz, 2 H, aryl H); 7.77 (d, $J$ = 8.3 Hz, 2 H, aryl-H); 9.94 (s, 1 H, *meso*-15 H); 10.15 (s, 2 H, *meso*-10 and *meso*-20 H). $^1$H NMR

(19) Lin, X. Q.; Kadish, K. M. *Anal. Chem.* **1985**, *57*, 1498–1501.

(300 MHz, D5-py) $\delta$ (ppm): −2.67 (s, 2 H, inner NH); 1.88 (t, 6 H, $J$ = 7.5 Hz, $CH_2\underline{CH_3}$); 2.66 (s, 6 H, $CH_3$); 3.42 (s, 6 H, $CH_3$); 3.48 (s, 6 H, $CH_3$); 3.95 (q, 4 H, $J$ = 7.5 Hz, $\underline{CH_2}CH_3$); 5.33 (s, 2 H, $NH_2$); 7.24 (d, 2 H, $J$ = 7.7 Hz, aryl-H); 7.76 (d, 2 H, $J$ = 7.7 Hz, aryl-H); 10.17 (s, 1 H, *meso*-15 H); 10.33 (s, 2 H, *meso*-10 and *meso*-20 H). MS (MALDI-TOF) $m/z$ = 542.04 $[M+H]^+$; 542.33 calcd for $C_{36}H_{40}N_5$. HRMS (ESI) $m/z$ = 542.3269 $[M+H]^+$; 542.3278 calcd for $C_{36}H_{40}N_5$; $m/z$ = 1083.6399 $[2M+H]^+$; 1083.6484 calcd for $C_{72}H_{79}N_{10}$.

**Synthesis of (13,17-Diethyl-2,3,7,8,12,18-hexamethyl-5-*p*-aminophenyl)-porphyrinato Zinc(II) 5.** Aminophenylporphyrin **4** (19 mg, 0.035 mmol), zinc(II) acetate dihydrate (120 mg, 0.55 mmol), and sodium acetate (90 mg, 1.10 mmol) were dissolved in chloroform (20 mL) and methanol (10 mL) and refluxed for 1 h. The solvent was removed, and the crude product was purified by chromatography over silica (dichloromethane). The front running red band was collected and led to zinc(II) aminophenylporphyrin **5** (18 mg, 85%) as a red microcrystalline solid. UV−vis ($CH_2Cl_2$) 333 (log $\varepsilon$, 4.33), 385sh (4.70), 406 (5.50), 500sh (3.47), 535 (4.20), 571 (4.13) nm. $^1$H NMR (300 MHz, $CDCl_3$) $\delta$ (ppm): 1.84 (t, $J$ = 7.3 Hz, 6 H, $CH_2\underline{CH_3}$); 2.49 (s, 6 H, $CH_3$); 3.50 (s, 6 H, $CH_3$); 3.57 (s, 6 H, $CH_3$); 3.97−4.05 (q, $J$ = 7.3 Hz, 4 H, $\underline{CH_2}CH_3$ overlapped with br s, 2 H, $NH_2$); 6.81 (d, $J$ = 8.2 Hz, 2 H, aryl-H); 7.67 (d, $J$ = 8.2 Hz, 2 H, aryl-H); 9.86 (s, 1 H, *meso*-15 H); 10.02 (s, 2 H, *meso*-10, *meso*-20 H). MS (MALDI-TOF) $m/z$ = 603.1 $[M]^{+\bullet}$ 603.2 calcd for $C_{36}H_{37}N_5Zn$. HRMS (ESI) $m/z$ = 603.2326 $[M]^{+\bullet}$, 603.2335 calcd for $C_{36}H_{37}N_5Zn$; 626.2221 $[M+Na]^+$, 626.2233 calcd for $C_{36}H_{37}N_5NaZn$; 1206.4604 $[2M]^+$, 1206.4675 calcd for $C_{72}H_{74}N_{10}Zn_2$.

**Synthesis of (13,17-Diethyl-2,3,7,8,12,18-hexamethyl-5-*p*-aminophenyl)-porphyrinato Copper(II) 6.** Aminophenylporphyrin **4** (24 mg, 0.04 mmol), copper(II) acetate monohydrate (124 mg, 0.62 mmol), and sodium acetate (130 mg, 1.58 mmol) were dissolved in chloroform (20 mL) and methanol (10 mL) and refluxed for 1 h. The solvent was removed, and the crude product was purified by chromatography over silica (dichloromethane). The front running red band was collected containing the copper(II) aminophenylporphyrin **6** (25 mg, 93%) as a red microcrystalline solid. UV−vis ($CH_2Cl_2$) 329 (log $\varepsilon$, 4.15), 382sh (4.60), 402 (5.44), 487sh (3.36), 528 (4.08), 564 (4.18) nm. MS (MALDI-TOF) $m/z$ = 602.0 $[M]^{+\bullet}$, 602.2 calcd for $C_{36}H_{37}CuN_5$. HRMS (ESI) $m/z$ = 602.2334 $[M]^{+\bullet}$, 602.2340 calcd for $C_{36}H_{37}CuN_5$; 1204.4628 $[2M]^+$, 1204.4685 calcd for $C_{72}H_{74}Cu_2N_{10}$.

**Synthesis of 1,8-Bis(13′,17′-diethyl-2′,3′,7′,8′,12′,18′-hexamethyl-5′-*p*-iminophenyl porphyrinyl)-3,6-di-*tert*-butyl-9*H*-carbazole 8.** Aminophenylporphyrin **4** (0.43 g, 0.79 mmol) and 1,8-diformyl-3,6-di-*tert*-butyl-9*H*-carbazole **7** (0.13 g, 0.39 mmol) were dissolved in degassed pyridine (125 mL), and the mixture was refluxed for 3 days. Then the solvent was removed, and the mixture was purified by column chromatography over silica gel (dichloromethane/methanol, 100/5). The main collected fraction afforded the bisporphyrin carbazole **8** (230.0 mg, 85%) as a brown microcrystalline solid. $^1$H NMR (300 MHz, D5-py) $\delta$ (ppm): −2.66 (br s, 4 H, inner NH); 1.35 (s, 18 H, *t*-butyl H); 1.74 (t, $J$ = 7.0 Hz, 12 H, $CH_2\underline{CH_3}$); 2.67 (s, 12 H, $CH_3$); 3.42 (s, 12 H, $CH_3$); 3.48 (s, 12 H, $CH_3$); 3.95 (q, $J$ = 7.0 Hz, 8 H, $\underline{CH_2}CH_3$); 7.24 (d, $J$ = 7.8 Hz, 4 H, aryl-H); 7.77 (d, $J$ = 7.8 Hz, 4 H, aryl-H); 8.01 (d, $J$ = 1.4 Hz, 2 H, linker H); 8.75 (d, $J$ = 1.9 Hz, 2 H, linker H); 10.17 (s, 2 H, $C\underline{H}$=N); 10.28 (s, 2 H, *meso*-15 H) ; 10.33 (s, 4 H, *meso*-10 and *meso*-20 H); 11.91 (br s, 1 H, linker NH). UV−vis ($CH_2Cl_2$) 332sh (log $\varepsilon$, 4.61), 404 (5.43), 502 (4.35), 537 (4.00), 571 (3.99), 625 (3.52) nm. MS (MALDI-TOF) $m/z$ = 1382.78 $[M+H]^+$, 1382.82 calcd for $C_{94}H_{100}N_{11}$. HRMS (ESI) $m/z$ = 1382.8099 $[M+H]^+$, 1382.8158 calcd for $C_{94}H_{100}N_{11}$; 1404.7929 $[M+Na]^+$, 1404.7977 calcd for $C_{94}H_{99}N_{11}Na$.

**Synthesis of 1,8-Bis[13′,17′-diethyl-2′,3′,7′,8′,12′,18′-hexamethyl-5′-*p*-imino-phenylporphyrinato)-zinc(II)]-3,6-di-*tert*-butyl-9*H*-carbazole 9.** Bisporphyrin carbazole **8** (60 mg, 0.01 mmol), zinc(II) acetate dihydrate (300 mg, 1.37 mmol) and sodium acetate (200 mg, 2.44 mmol) were dissolved in chloroform (50 mL) and methanol (25 mL) and refluxed for 10 min. The solvent was removed, and the crude product was purified by chromatography over silica (dichloromethane/heptane, 70/30). The front running red band was collected, and the solvent was removed to give bis-zinc(II) bisporphyrin carbazole **9** (55 mg, 84%) as a red microcrystalline solid. UV−vis ($CH_2Cl_2$): 333 (log $\varepsilon$, 4.89), 405 (5.87), 469sh (3.80), 535 (4.63), 571 (4.56), 740 (2.75) nm. $^1$H NMR (300 MHz, $CDCl_3$) $\delta$ (ppm): 1.65 (s, 18 H, *t*-butyl H); 1.83 (t, $J$ = 7.8 Hz, 12 H, $CH_2\underline{CH_3}$); 2.59 (s, 12 H, $CH_3$ ($\beta$3 and 7)); 2.87 (s, 12 H, $CH_3$ ($\beta$12 and 18)); 3.38 (s, 12 H, $CH_3$ ($\beta$2 and 8)); 3.93−4.01 (q, $J$ = 7.8 Hz, 8 H, $\underline{CH_2}CH_3$); 7.96 (d, $J$ = 8.0 Hz, 4 H, aryl-H); 8.18 (d, $J$ = 8.0 Hz, 4 H, aryl-H); 8.02 (d, $J$ = 1.4 Hz, 2 H, linker H); 8.47 (d, $J$ = 1.4 Hz, 2 H, linker H); 9.33 (s, 2 H, *meso*-15 H); 9.70 (s, 4 H, *meso*-10 and *meso*-20 H); 9.87 (2 H, s, -C$\underline{H}$N-); 13.19 (1 H, s, linker NH). MS (MALDI-TOF) $m/z$ = 1505.7 $[M]^{+\bullet}$, 1505.6 calcd for $C_{94}H_{95}N_{11}Zn_2$. HRMS (ESI) $m/z$ = 1506.6347 $[M+H]^+$, 1506.6428 calcd for $C_{94}H_{96}N_{11}Zn_2$; 1528.6261 $[M+Na]^+$, 1528.6247 calcd for $C_{94}H_{95}N_{11}NaZn_2$.

**Synthesis of [1,8-Bis[13′,17′-diethyl-2′,3′,7′,8′,12′,18′-hexamethyl-5′-*p*-iminophenyl porphyrinato)-copper(II)]-3,6-di-*tert*-butyl-9*H*-carbazolide]-CuOAc 10.** Bisporphyrin carbazole **8** (27 mg, 0.02 mmol), copper(II) acetate monohydrate (140 mg, 0.61 mmol) and sodium acetate (84 mg, 1.02 mmol) were dissolved in chloroform (20 mL) and methanol (10 mL) and heated at reflux for 10 min. The reaction mixture was then diluted with dichloromethane (40 mL), washed with water (3 × 100 mL) and the solvent was removed. Recrystallization of the obtained product from dichloromethane/methanol solution affords the tris-copper(II) bisporphyrin carbazole **10** (30 mg, 98%) as a red microcrystalline solid. UV−vis ($CH_2Cl_2$) 330 (log $\varepsilon$ 4.59), 401 (5.64), 454sh (4.37), 528 (4.36), 564 (4.44) nm. MS (MALDI-TOF) $m/z$ = 1565.4 $[M-X]^+$ 1565.6 calcd for $C_{94}H_{94}Cu_3N_{11}$. HRMS (ESI) $m/z$ = 1565.5568 $[M-X]^+$, 1565.5576 calcd for $C_{94}H_{94}Cu_3N_{11}$.

**Synthesis of 1,8-Bis[13′,17′-diethyl-2′,3′,7′,8′,12′,18′-hexamethyl-5′-*p*-iminophenyl porphyrinato)-copper(II)]-3,6-di-*tert*-butyl-9*H*-carbazole 11.** A mixture of copper(II) aminophenylporphyrin **6** (50 mg, 0.08 mmol) and carbazole **7** (14 mg, 0.04 mmol) were refluxed in 20 mL for 3 days and then evaporated under vacuum. The residue was then chromatographed over silica gel and eluted with dichloromethane. The first eluting band afforded the bis-copper bisporphyrin carbazole **11** (60 mg, 97%) as a pure solid. UV−vis ($CH_2Cl_2$) 401 (log $\varepsilon$ 5.12), 537 (3.81), 563 (4.01) nm. HRMS (MALDI/TOF) $m/z$ = 1503.6324 $[M-X]^+$, 1503.6358 calcd for $C_{94}H_{95}Cu_2N_{11}$.

**Synthesis of 1,8-Bis[13′,17′-diethyl-2′,3′,7′,8′,12′,18′-hexamethyl-5′-*p*-imino-phenylporphyrinato)-zinc(II)]-3,6-di-*tert*-butyl-9*H*-carbazolide-CuOAc 12.** To a solution of bis-zinc(II) bisporphyrin carbazole **9** (137 mg, 0.09 mmol) in 1,2-dichloroethane (50 mL) were added copper(II) acetate hydrate (365 mg, 1.83 mmol) and sodium acetate (303 mg, 3.69 mmol) in methanol (25 mL). After 2 h refluxing, the reaction mixture was extracted with 50 mL of dichloromethane. The organic layer was then washed with water (3 × 100 mL), dried over $MgSO_4$ and evaporated. The solid residue was then taken with dichloromethane and precipitated with heptane giving copper(II) bis-zinc(II) bisporphyrin carbazole **12** (91 mg, 64%). UV−vis ($CH_2Cl_2$) 402 (log $\varepsilon$, 5.58), 532 (4.25), 567 (4.25) nm. MS (MALDI-TOF) $m/z$ = 1567.36 $[M-X]^+$, 1567.56 calcd for $C_{94}H_{94}CuN_{11}Zn_2$. HRMS (ESI) $m/z$ = 1567.5503 $[M-X]^+$, 1567.5567 calcd for $C_{94}H_{94}CuN_{11}Zn_2$.

**Synthesis of (1,8-Diphenylimino-3,6-di-*tert*-butylcarbazolide)-copper(II) Acetate 14.** An analytical sample of **14** was synthesized from 1 equiv of 1,8-diphenylimino-3,6-di-*tert*-butylcarbazole dissolved in chloroform, by addition of a methanol solution of 10 equiv of copper(II) acetate hydrate and 20 equiv of anhydrous sodium acetate. The mixture was refluxed for 45 min, extracted with dichloromethane, washed with water, dried over $MgSO_4$. After evaporation the resulting solid was crystallized from a dichloromethane/pentane mixture leading almost

quantitatively to **14**. UV−vis ($CH_2Cl_2$) 438 (log $\varepsilon$, 4.54) nm. MS (MALDI-TOF) $m/z$ = 546.946 $[M-OAc]^+$, 547.204 calcd for $C_{34}H_{34}CuN_3$.

**Synthesis of (1,8-Diphenylimino-3,6-di-*tert*-butylcarbazolide)-copper(II) Chloride 15.** An analytical sample of **15** was obtained by dissolving 11 mg (17 $\mu$mol) in 5 mL of $CH_2Cl_2$. To this solution were added 10 mL of a saturated solution of NaCl in water. The resulting mixture was stirred for 3 h. The organic layer was then isolated and evaporated to afford **15** (10 mg, 99%). UV−vis ($CH_2Cl_2$) 445 (log $\varepsilon$, 4.15) nm. MS (MALDI-TOF) $m/z$ = 546.897 $[M-Cl]^+$, 547.204 calcd for $C_{34}H_{34}CuN_3$.

## Conclusion

In conclusion, the straightforward, scalable (in grams) synthesis of a new dimer porphyrin **8** is described, which is used to prepare in high yield new bis- and tris-metalated dimers that represent good candidates for catalysis, energy transfer, electrochemistry, and other physical studies. It is also possible to incorporate other metals into both the porphyrin core and the bridge. Moreover, the same synthetic route can be used with other amino porphyrins or amino corroles as well as other bridges such as 1,8-diformyl-dibenzofuran, for example. Dimeric species can also be obtained under these conditions.

The synthesized bis-metal and tris-metal dyads were electrochemically and spectroscopically characterized in several nonaqueous solvents, and their redox behavior is compared to that of the unlinked carbazoles and unlinked porphyrins, after which mechanisms and electron transfer sites are proposed. In most, but not all cases, the tris-metal dyads show a splitting of the first oxidation and first reduction. The binding constants of the Zn compounds with $OAc^-$ and $Cl^-$ ligands are evaluated. In addition, it is seen that the carbazole bridge Cu ion of the tris-metal dyads enhances the $\pi-\pi$ (ring−ring) interaction between the two porphyrin units as compared to the case of the bis-metal dyads.

**Acknowledgment.** The Burgundy Council is acknowledged for postdoctoral fellowship to T. Khoury, the Centre National de Recherche Scientifique (CNRS; UMR 5260), and the Robert A. Welch Foundation (K.M.K., Grant E-680) for research funding. The Centre National de Recherche Scientifique (CNRS) is also acknowledged for Ph.D. support grant for B.H. The authors thank Dr. S. Brandès for recording ESR spectra.

**Supporting Information Available:** One figure (Figure S1) and one Table (Table S1) of HRMS-ESI mass spectral data and ESR parameters of Cu compounds respectively, table of half-wave and peak potentials in PhCN and pyridine (Table S2), two figures showing views of X-ray structure for the chloro derivative of **10** (Figures S2 and S3), two figures showing cyclic voltammograms of **9** and **12** in $CH_2Cl_2$ containing 0.1 M TBACl or TBA(OAc) (Figures S4 and S5) and four figures showing UV−visible spectra of the Zn compounds under different solution conditions (Figures S6 to S9). Figure S10 presents the $^1H$ NMR spectra of the free-base and zinc porphyrin derivatives and Figure S11 gives cyclic voltammograms of the copper dyads in pyridine. This material is available free of charge via the Internet at http://pubs.acs.org.